Chinese Chemical Letters 35 (2024) 108493

Contents lists available at ScienceDirect

Chinese Chemical Letters

journal homepage: www.elsevier.com/locate/cclet

J-aggregation of photosensitizers leads to an ultrahigh drug-loading system for targeted delivery

Yun Qu[1], Wenjuan Jin[1], Yichen Wan, Zhichao Pei, Yuxin Pei*

College of Chemistry & Pharmacy, Northwest A&F University, Yangling 712100, China

ARTICLE INFO

Article history:
Received 17 November 2022
Revised 16 April 2023
Accepted 20 April 2023
Available online 23 April 2023

Keywords:
J-aggregate
Ultrahigh drug-loading
Aza-BODIPY
Hollow MnO_2
Phototherapy
Pillar[*n*]arene

ABSTRACT

Drug loading capacity is very important in the construction of targeted drug delivery systems (TDDSs) for the improvement of drug delivery efficiency. However, the drug-loading capacity of most nanomaterials is non-idealistic, and developing the high drug-loading TDDSs is still a critical challenge. In this work, an ultrahigh loading system (denoted as HMPB2) was prepared *via* J-aggregation of an aza-boron dipyrromethene derivative (Bod) by using hollow MnO_2 modified with glucosamine pillar[5]arene as a carrier, which was demonstrated to have typical J-aggregate absorption of Bod, specific cancer cells targeting ability, negligible dark cytotoxicity, and potent phototoxicity. This work provides a successful example to construct an ultrahigh drug-loading system *via* J-aggregation for targeted delivery.

© 2023 Published by Elsevier B.V. on behalf of Chinese Chemical Society and Institute of Materia Medica, Chinese Academy of Medical Sciences.

Drawbacks of most therapeutic agents, including poor water solubility, lack of targeting, low delivery efficiency, and bioavailability, hamper their bio-application [1,2]. Targeted drug delivery systems (TDDSs) based on nanomaterials can improve drug delivery efficiency, prolong circulation time, and reduce systemic toxicity, therefore possessing great clinical promise [3–7]. An increasing realization is that drug loading capacity and delivery efficiency have considerable importance in the construction of TDDSs [8,9]. Specifically, compared with relatively low drug-loading systems, a high drug-loading system can achieve a satisfactory therapeutic effect with a low dose of nanomaterials which in excess may bring side effects [10]. Therefore, the suboptimal drug-loading capacity of most nanomaterials currently highlights the necessity to develop high drug-loading TDDSs.

As a newly emerging structure of manganese oxides, hollow MnO_2 (HM) inherits the attractive characteristics of manganese oxides nanomaterials, including glutathione consumption, oxygen production, biodegradation, and magnetic resonance imaging [11,12]. Importantly, HM possesses an enormous cavity to load cargo, which is an ideal candidate to realize ultrahigh loading of cargo [13,14]. However, there are few reports about maximizing the drug-loading potential for improving therapeutic efficacy.

J-aggregates of organic dyes, a self-assembling state with a regular slipped packing arrangement, have been widely utilized in biological applications due to narrow red-shifted absorption/emission bands compared with their monomers [15,16]. Classic organic dyes which can form J-aggregates include porphyrin derivatives, squaraine dyes, boron dipyrromethenes (BODIPY), *etc.* [17–19]. Among them, J-aggregates of BODIPY and aza-boron dipyrromethenes (aza-BODIPY) with high fluorescence quantum yield, excellent photothermal conversion efficiency and singlet oxygen quantum yield, good chemical/optical stability, and ease of modification, have attracted much attention for near-infrared (NIR) bioimaging and phototherapy [16,20,21]. Intriguingly, we envision that the J-aggregation of therapeutic agents in TDDSs may improve the drug loading capacity and prevent premature drug leakage through translating monomers into J-aggregates in the large cavity of hollow nanomaterials.

In the past ten years, the functional pillar[*n*]arene used in drug delivery has gained more and more attention for its facility to improve hydrophilicity, targeting, biocompatibility, and efficiency of various nanocarriers (*e.g.*, polymers, metal-organic framework, inorganic porous materials) by the surface modification of supramolecular chemistry [22–29]. Herein, considering the negatively charged surface of HM, a positively charged hydrophilic targeting macromolecule glucosamine pillar[5]arene (NP5) was first synthesized and modified on the surface of HM through electrostatic interaction to form HMP. After that, aza-BODIPY derivative (Bod) was loaded into the large cavity of HMP to fabricate HMPB2. We expected HMPB2 would demonstrate ultrahigh drug-loading capacity, typical J-aggregate absorption of Bod, specific cancer cell targeting ability stemming from the Warburg

* Corresponding author.
E-mail address: peiyx@nwafu.edu.cn (Y. Pei).
[1] These authors contributed equally to this work.

https://doi.org/10.1016/j.cclet.2023.108493
1001-8417/© 2023 Published by Elsevier B.V. on behalf of Chinese Chemical Society and Institute of Materia Medica, Chinese Academy of Medical Sciences.

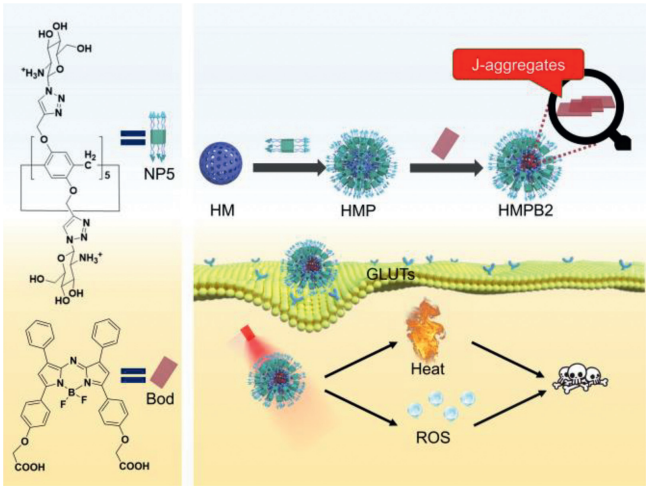

Scheme 1. A scheme indicating the construction of HMPB2 and its application for phototherapy.

effect [30], and good phototoxicity under NIR laser irradiation (Scheme 1).

The synthetic process of NP5 was presented in Fig. S1 (Supporting information). HM with an average size of 251 nm and zeta potential of −26.6 mV (Figs. 1a and b) was prepared [14]. Transmission electron microscopy (TEM) images demonstrate HM possesses a hollow structure (Fig. 1c). Furthermore, positive-charged NP5 was modified onto the surface of HM through electrostatic interaction, yielding HMP with elevated zeta potential and rough surface, which was then applied as a hydrophilic targeting carrier. The successful modification of NP5 on the surface of HM was further proved by ultraviolet-visible (UV–vis) spectroscopy. The typical peak of NP5 at 291 nm was observed in the UV–vis spectrum of HMP (Fig. 1d).

To prove the formation of J-aggregates, Bod aqueous solution was prepared. Unsurprisingly, the Tyndall effect was observed (Fig. S10a in Supporting information), which suggested the presence of nanoparticles (BodNPs). Dynamic light scattering (DLS) and TEM were then performed to investigate the size and morphology of BodNPs. DLS analysis showed that the average size of BodNPs was 187 nm with a zeta potential of −21.6 mV (Fig. S10b in Supporting information), and TEM images disclosed a regular structure of BodNPs (Fig. S10c in Supporting information). Furthermore, a strong red-shift narrow peak at 799 nm appeared on the UV–vis spectrum of BodNPs compared with that of Bod, which was consistent with the characteristics of Bod's J-aggregates (Fig. 1d). These results confirmed that Bod formed J-aggregates in water.

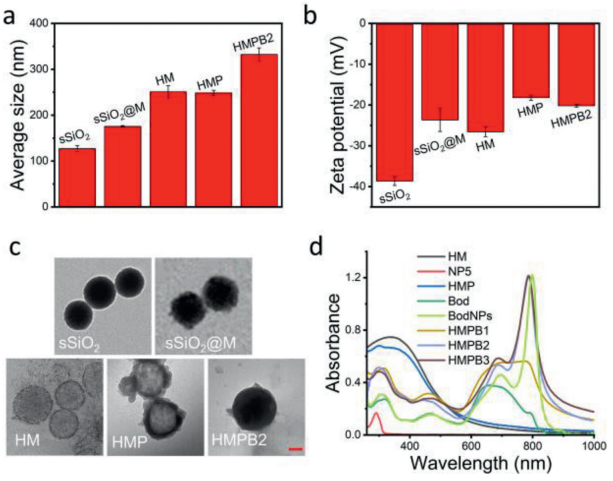

Fig. 1. (a) The average size distribution and (b) zeta potential of different nanoparticles (n=3). (c) The TEM images of different nanoparticles (scale bar: 50 nm). (d) The UV–vis spectra of HM, NP5, HMP, Bod, BodNPs, HMPB1, HMPB2, and HMPB3 in water.

Subsequently, Bod loading of HMP was investigated. To maximize the drug loading potential of HMP, multiple loading processes of Bod were studied during the preparation of HMPB1 *via* UV–vis spectroscopy. The single loading efficiency decreased by degrees during six loading circles (Fig. S11 in Supporting information), indicating the loading capacity of HMP reached saturation gradually. The total loading efficiency and loading capacity of HMPB1 were 92.3% and 84.7%, respectively (Table S1 in Supporting information). Next, the loading potential of HMP under different weight ratios (Bod: HMP) was studied in a single loading process (Table S1 in Supporting information). When the weight ratio was 6:1 (HMPB2), the loading efficiency and loading capacity of Bod were 87.6% and 84.0%, respectively. When the weight ratio was 8:1 (HMPB3), the loading efficiency decreased to 74.2%, while the loading capacity only increased by 1.6%. As shown in Fig. 1d, the wide absorption band at 600–800 nm of HMPB1 demonstrated the successful loading of Bod. The typical peaks of BodNPs were observed in the UV–vis spectra of HMPB2 and HMPB3, demonstrating the successful loading of Bod. It is reasonable to speculate that Bod exists in the form of BodNPs in HMPB2 and HMPB3, while there may be a slight aggregation phenomenon in HMPB1. Compared with HMPB1 and HMPB3, HMPB2 has stronger absorption at 808 nm with the lower Bod feeding weight ratio, which was herein selected for further experiments. Moreover, TEM images showed that there were obvious dark areas in the interior of HMPB2, which indicates that Bod is located in the HM cavity rather than attached to the surface (Fig. 1c and Fig. S12 in Supporting information).

For further bio-application, the particle size stability of HMPB2 and the stability of J-aggregates in HMPB2 were investigated *via* DLS and UV–vis spectroscopy, respectively. DLS results showed that HMPB2 possessed good particle size stability in PBS containing 10% fetal bovine serum (FBS) and complete medium (Fig. S13 in Supporting information). In addition, UV–vis spectra revealed that there was no obvious change in water and phosphate buffer saline (PBS, pH 5.4) after storage for different time intervals, suggesting good stability of J-aggregates in HMPB2 (Figs. S14a and b in Supporting information). However, the absorbance of HMPB2 at 799 nm reduced to 70.0%, 52.9% and 49.4% with the increase of storage time and pH value in the pH range 6.0–7.4, respectively (Figs. S14c-e in Supporting information). To clarify this phenomenon, the absorbance of HMPB2 in NaCl aqueous solution was studied, where the Na^+ concentration was equal to that of PBS. The absorbance also decreased to 57.0% after 24 h (Fig. S14f in Supporting information). These results indicated the disaggregation of J-aggregates in HMPB2 gradually under physiological conditions.

The photothermal and photodynamic properties of HMPB2 were measured under irradiation. When Bod concentration was 40 μg/mL, the temperature increments were 33.7 °C and 26.8 °C under 808 nm or 685 nm laser irradiation, respectively (Figs. 2a and b). This showed that the photothermal conversion ability of HMPB2 under 808 nm was superior to that of 685 nm, which was validated by photothermal conversion efficiency of 808 nm (47.3%) and 685 nm (21.3%) calculated according to the reported literature, respectively [31]. Additionally, there was no obvious temperature variation even after five heating-cooling cycles, suggesting good photothermal stability of HMPB2 (Fig. 2c). The ROS generation was studied using 1,3-diphenylisobenzofuran (DPBF) as an indicator. As shown in Fig. 2d, the absorption of DPBF at 473 nm showed a slight decline without irradiation. However, a rapid decrease in the 685 nm group was observed, which was superior to

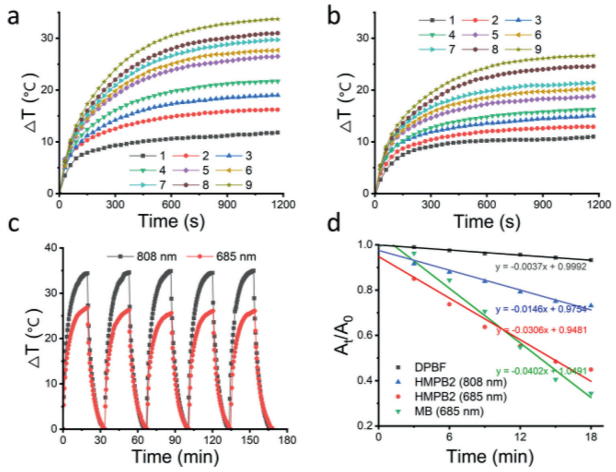

Fig. 2. Photothermal heating curves of HMPB2 under (a) 808 nm and (b) 685 nm laser irradiation (130 mW/cm^2). For (a) and (b), the Bod concentrations of groups 1–9 were 0, 1, 3, 5, 10, 15, 20, 30, and 40 μg/mL, respectively. (c) Photothermal heating-cooling curves of HMPB2 (Bod: 40 μg/mL) upon NIR exposure. (d) ROS generation measurement of HMPB2 by DPBF in water (80 mW/cm^2).

the 808 nm group, suggesting a stronger ROS generation capacity of HMPB2 under 685 nm laser irradiation where the singlet oxygen quantum yield was determined to be 0.18, using methylene blue as the standard photosensitizer [32]. Considering the unsatisfying stability of J-aggregates in HMPB2 under physiological conditions, 685 nm is a more appropriate wavelength for phototherapy. And the final cytotoxicity was derived from the synergistic photothermal and photodynamic effect of Bod under 685 nm.

The cellular uptake and targeting ability were investigated by flow cytometry. To meet the proliferation of cancer cells, glucose transporters (GLUTs) are ubiquitously overexpressed in various cancer cells, which was explored to strengthen the targeting ability of TDDS towards cancer cells [30,33]. As shown in Fig. 3a, the fluorescence intensity in HepG2 cells increased with incubation time, indicating a time-dependent cellular uptake of HMPB2. To identify the targeting ability, the cellular uptake of HMPB2 in various cancer cells (HeLa, HepG2, 4T1), as well as normal HL7702 cells, was tested. As shown in Fig. 3b, the fluorescence intensity of HMPB2 in Phl (phloretin, GLUTs inhibitor) pre-treated HepG2, HeLa, and 4T1 cells reduced compared to the corresponding HMPB2 group, indicating GLUTs-mediated specific targeting ability, which was consistent with the results reported in the literature [34]. In addition, the fluorescence intensity in HL7702 cells was significantly lower than those of the cancer cells, which further confirmed the targeting ability of HMPB2 to cancer cells.

The intracellular ROS generation of HMPB2 was detected by confocal laser scanning microscopy (CLSM) using 2′,7′-dichlorodihydrofluorescein diacetate (DCFH-DA) as ROS fluorescent probe. Compared with the PBS and dark groups, strong fluorescence was observed under 685 nm laser irradiation, slightly higher than that of 808 nm group (Figs. 3c and d, Fig. S17 in Supporting information). Moreover, the fluorescence intensity of sodium ascorbate (VcNa, ROS scavenger) treated groups was both weakened. These results indicated abundant ROS generation in HepG2 cells treated with HMPB2 under irradiation. Additionally, the ROS generation ability under 808 nm laser irradiation was attenuated with incubation time extension caused by the non-ideal stability of BodNPs in HMPB2 (Fig. 3d).

The biocompatibility and cytotoxicity were examined *via* bromidemethyl tetrazolium (MTT) assay. The increment of the loading capacity of TDDS can reduce the dosage of carriers to avoid the side effects caused by excess carriers. With the increase concentration of HMP, an apparent decrease in the survival rate of HepG2

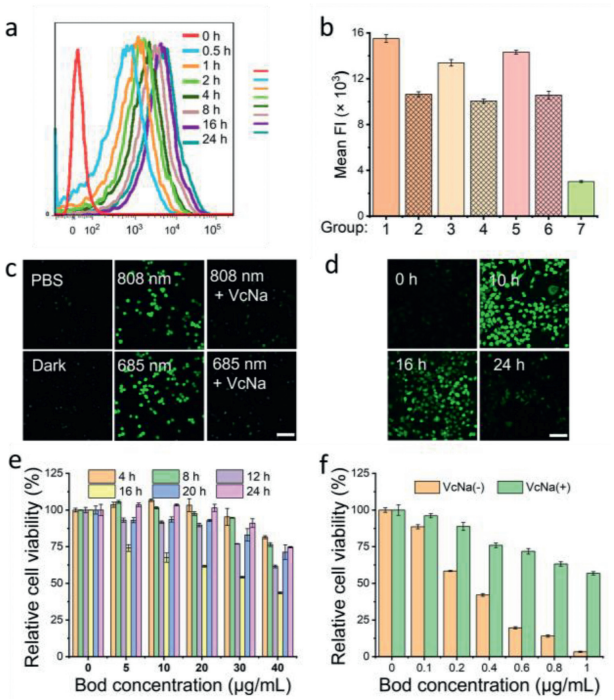

Fig. 3. (a) Cellular uptake of HMPB2 in HepG2 cells with different incubation times. (b) Targeting ability of HMPB2 was detected by flow cytometry (1–7: HepG2, HepG2 + Phl, HeLa, HeLa + Phl, 4T1, 4T1 + Phl, HL7702, respectively) (n=3). ROS generation in HepG2 cells (c) with different treatments at 6 h and (d) with different incubation times under 808 nm laser irradiation (scale bar: 100 μm). The relative cell viability of HepG2 cells incubated with HMPB2 (e) for 4, 8, 12, 16, 20, 24 h upon 808 nm irradiation and (f) for 16 h upon 685 nm irradiation (808 nm, 80 mW/cm^2, 30 min; 685 nm, 80 mW/cm^2, 30 min) (n=5).

and HL7702 cells was observed (Fig. S18a in Supporting information), suggesting the unfavorable biological safety at a high concentration. In contrast, HMPB2 showed negligible dark cytotoxicity and the cell survival rate remained above 95% at a high Bod concentration (40 μg/mL), which could be attributed to the low content of HMP (Fig. S18b in Supporting information).

Next, the phototoxicity of HMPB2 under different conditions was investigated. As shown in Fig. 3e, HepG2 cells treated with HMPB2 for 16 h showed the lowest cell viability under 808 nm laser irradiation (43.5%, 40 μg/mL). Meanwhile, no obvious cell death was observed in BodNPs treated group upon 808 nm irradiation (Fig. S19b in Supporting information). These results indicated that the weak cytotoxicity of HMPB2 under 808 nm may be attributed to the disaggregation of Bod J-aggregation in physiological conditions. By contrast, the survival rate of the 685 nm group dropped to 2.3% with a low Bod concentration (5 μg/mL) (Fig. S19a in Supporting information), which can be attributed to the stable absorbance of HMPB2 at 685 nm whether the Bod was in monomer or J-aggregate form. Next, we subsequently narrowed the concentration to a range of 0–1 μg/mL. As displayed in Fig. 3f, HMPB2 exhibited apparent concentration-dependent cytotoxicity, where the half-maximal inhibitory concentration (IC_{50}) in HepG2 cells with or without VcNa pre-incubation was 1.1 and 0.4 μg/mL, respectively. Altogether, these results showed that HMPB2 could improve the stability of BodNPs to a certain extent. Although the therapeutic efficiency of HMPB2 under irradiation of 808 nm was much weaker than that of 685 nm, we believe that highly efficient phototherapy with a red-shift NIR window would be expected to realize by optimizing systems.

In conclusion, we constructed an ultrahigh loading system (HMPB2) *via* J-aggregation of Bod by using HM modified with glucosamine pillar[5]arene as a carrier. HMPB2 showed good

photothermal conversion efficiency and abundant ROS generation ability under NIR laser irradiation. Flow cytometry analysis proved the specific targeting ability of HMPB2 due to the overexpressed GLUTs on the cancer cell membrane. The negligible dark toxicity and excellent cytotoxicity to cancer cells under 685 nm irradiation were shown *in vitro*. This work affords a good example to construct an ultrahigh drug-loading system *via* J-aggregation for targeted delivery, inspiring further exploration on hollow nanomaterials mediated co-delivery of other types of dyes possessing J-aggregate properties and immune adjuvant to improve the anti-tumor effect [35–38].

Declaration of competing interest

The authors declare that they have no known competing financial interests or personal relationships that could have appeared to influence the work reported in this paper.

Acknowledgments

This work was supported by the National Natural Science Foundation of China (Nos. 22171230 and 21877088) and the Project of Science and Technology of Social Development in Shaanxi Province (No. 2021SF-120). The authors thank Life Science Research Core Services (LSRCS), Northwest A&F University for helping with characterizations. The authors would like to thank Shiyanjia Lab (www.shiyanjia.com) for the TEM analysis.

Supplementary materials

Supplementary material associated with this article can be found, in the online version, at doi:10.1016/j.cclet.2023.108493.

References

[1] W. Feng, Y. Lv, Z. Chen, et al., Chem. Eng. J. 417 (2021) 129178.
[2] S. Senapati, A.K. Mahanta, S. Kumar, P. Maiti, Signal Transduct Target. Ther. 3 (2018) 7.
[3] X. Hu, L. Gao, S. Mosel, et al., Small 14 (2018) 1803952.
[4] C. Yao, P. Wang, X. Li, et al., Adv. Mater. 28 (2016) 9341–9348.
[5] R. Sun, J. Dai, M. Ling, et al., J. Nanobiotechnol. 20 (2022) 194.
[6] C. Sun, Z. Wang, K. Yang, et al., Small 17 (2021) 2101139.
[7] Y. Wang, M. Jin, Z. Chen, et al., Chem. Commun. 56 (2020) 10642–10645.
[8] H. Zhang, L. Zhang, Z. Cao, et al., Small 18 (2022) 2200299.
[9] X. Sun, G. He, C. Xiong, et al., ACS Appl. Mater. Interfaces 13 (2021) 3679–3693.
[10] Y. Liu, G. Yang, T. Baby, et al., Angew. Chem. Int. Ed. 59 (2020) 4720–4728.
[11] W. Xu, X. Qing, S. Liu, et al., Small 18 (2022) 2106511.
[12] Y. Wang, Y. Li, Z. Zhang, et al., Adv. Mater. 33 (2021) 2103748.
[13] X. Xu, J. Duan, Y. Liu, et al., Acta Biomater. 126 (2021) 445–462.
[14] G. Yang, L. Xu, Y. Chao, et al., Nat. Commun. 8 (2017) 902.
[15] F. Wurthner, T.E. Kaiser, C.R. Saha-Moller, Angew. Chem. Int. Ed. 50 (2011) 3376–3410.
[16] X. Bao, S. Zheng, L. Zhang, et al., Angew. Chem. Int. Ed. 61 (2022) e202207250.
[17] Q. Liu, Q. Jia, J. Zhu, et al., Chin. Chem. Lett. 25 (2014) 752–756.
[18] P. Sun, Q. Wu, X. Sun, et al., Chem. Commun. 54 (2018) 13395–13398.
[19] S. Xu, H. Liu, S. Huan, L. Yuan, X. Zhang, Mater. Chem. Front. 5 (2021) 1076–1089.
[20] Y. Liu, C. Xu, L. Teng, et al., Chem. Commun. 56 (2020) 1956–1959.
[21] Y. Zhu, W. Lin, W. Zhang, et al., Chin. Chem. Lett. 28 (2017) 1875–1877.
[22] W. Qian, M. Zuo, P. Niu, X. Hu, L. Wang, Chin. Chem. Lett. 33 (2022) 1975–1978.
[23] Yu G, M. Xue, Z. Zhang, et al., J. Am. Chem. Soc. 134 (2012) 13248–13251.
[24] M. Wu, J. Gao, F. Wang, et al., Small 14 (2018) 1704440.
[25] T. Xiao, W. Zhong, L. Xu, et al., Org. Biomol. Chem. 17 (2019) 1336–1350.
[26] X.Y. Lou, Y.W. Yang, Adv. Mater. 32 (2020) 2003263.
[27] H. Zheng, L. Fu, J. Jiao, et al., Nat. Commun. 17 (2019) 1336–1350.
[28] Z. Shen, N. Ma, F. Wang, et al., Chin. Chem. Lett. 33 (2022) 4563–4566.
[29] Y. Chang, K. Yang, P. Wei, et al., Angew. Chem. Int. Ed. 53 (2014) 13126–13130.
[30] K. Narayanan, N. Erathodiyil, B. Gopalan, et al., Adv. Healthcare Mater. 5 (2016) 696–701.
[31] W. Ren, Y. Yan, L. Zeng, et al., Adv. Healthcare Mater. 14 (2023) 590.
[32] Z. Ruan, Y. Zhao, P. Yuan, et al., J. Mater. Chem. B 6 (2018) 753–762.
[33] Q. He, I. Minn, Q. Wang, et al., Angew. Chem. Int. Ed. 55 (2016) 12035–12039.
[34] Y. Wang, J. Li, Z. Chen, et al., Chem. Commun. 58 (2022) 3945–3948.
[35] Q. Han, C. Wang, Z. Li, et al., Anal. Chem. 92 (2020) 3324–3331.
[36] Y. Li, T. Ma, H. Jiang, et al., Angew. Chem. Int. Ed. 61 (2022) e202203093.
[37] P. Sun, Q. Wu, X. Sun, et al., Chem. Commun. 54 (2018) 13395.
[38] N. Yu, M. Ding, F. Wang, Nano Today 46 (2022) 101600.